Transactions, SMiRT-24
BEXCO, Busan, Korea - August 20-25, 2017
Division VI
Paper ID: 06-18-03

Experimental Studies on Modular Steel-Concrete Construction Assembled with a Novel Fabrication Technology

Kadir C. Sener[1], Amit H. Varma[2], Sijia Wang[3], Saahastaranshu R. Bhardwaj[4], Stewart Gallocher[5]

[1] Research Engineer, Civil Engineering, Purdue University, West Lafayette, IN, USA
[2] Professor, Civil Engineering, Purdue University, West Lafayette, IN, USA
[3] Graduate Student, Civil Engineering, Purdue University, West Lafayette, IN, USA
[4] Ph.D. Student, Civil Engineering, Purdue University, West Lafayette, IN, USA
[5] Structural Engineer, Director, Modular Walling Systems Ltd., Glasgow, Scotland, UK

ABSTRACT

Several nuclear vendors have started to rollout design solutions for Nuclear Power Reactors (NPRs) and Small Modular Reactors (SMRs) that implement modular construction technologies as a key component. Modular fabrication technologies can be utilized within and outside the reactor containment boundaries. While there are numerous existing in-house technologies that enable the construction of Steel-Concrete Composite (SC) modular walls and floors, most of the available systems are complex to design, fabricate and construct. A novel technology is introduced that solves many of the challenges presented by SC modular construction whilst retaining the benefits. Experimental evaluations have been performed to demonstrate the construction quality, and robust structural performance of the modular fabrication technology. This paper presents the experimental results obtained from SC beam specimens constructed using the novel modular fabrication technology. The specimen behavior was consistent with the intended design philosophy, and the fabrication performance was satisfactory. The specimens had out-of-plane shear failure in concrete without any premature failure mode in the modules or the welded joints. The failure strengths were also estimated accurately and conservatively by relevant design code equations.

INTRODUCTION

This paper presents the experimental evaluations conducted on steel-concrete composite (SC) walls constructed using a novel fabrication technology. The experiments involved subjecting the modular panels to out-of-plane shear loading. The test objective was to conduct out-of-plane bending tests on two orthogonal unit widths of a typical modular SC design configuration. The unit widths were defined based on the transverse (or longitudinal) spacing between the SC beam shear reinforcement (diaphragm or inner plates). The diaphragm plates were located at the center of the unit widths. The size and number of shear studs on the faceplates was designed to conform the stud requirements provided in AISC N690s1.

The out-of-plane shear tests were conducted by subjecting the specimens to four-point bending . The load magnitudes at the two loading locations were controlled using a single hydraulic pump, thus ensuring the loads in two spans were within tolerance of about 5%. The loading was applied quasi-statically. Additionally, several loading-unloading cycles were conducted before the final load push to failure. The experimental results include the applied load vs. (i) mid-span displacement response of the specimen, (ii) strains measured on faceplates and diaphragm (inner) plates, and (iii) rotations measured at load and support locations.

The first objective of this testing program was to experimentally investigate the robustness and quality of the fabrication technique by verifying the performance of the steel modules and their connections . The second objective was to evaluate the out-of-plane shear and flexure strength of the specimens, and compare the experimental results with the strength equations provided in relevant design codes to confirm the applicability of code design provisions.

FABRICATION OF STEEL MODULES

The specimens were fabricated with a new concept that improves construction schedule by ensuring rapid fabrication and assembly of the modules. The fabrication sequence is illustrated in Figure 1. The modules consist of individual U-shaped bricks that are fabricated by; (i) either cutting the steel plate to desired shape or fabricating the complete section, (ii) folding the steel plate in press to create an L-Shaped section (or U-shaped brick), (iii) welding shear studs to the inside of the plates, and (iv) assembling wall or flooring members by welding the individual L-shaped or U-shaped units (bricks). The tested specimens were fabricated from steel plates that were folded to form the faceplates and diaphragm (inner) plates. Two identical folded sections were then welded at the diaphragms to form the final shape of the specimen.

This novel way of assembling modular wall and flooring units (bricks) has significant design advantages; such as, (i) bricks can be fabricated quickly to achieve straight, curved, corner wall and floor section configurations, (ii) there is no restriction on the module thickness as individual 'bricks' can be obtained by folding plates (6mm to 25mm thick), (iii) shear capacity of the basic unit (brick) exceeds the the capacity of conventional modules that incorporate tie bars, (iv) the ability to connect directly onto the diaphragms enhances fabrication and mitigates some of the difficulties encountered with current systems, particularly at interfaces with RC sections.

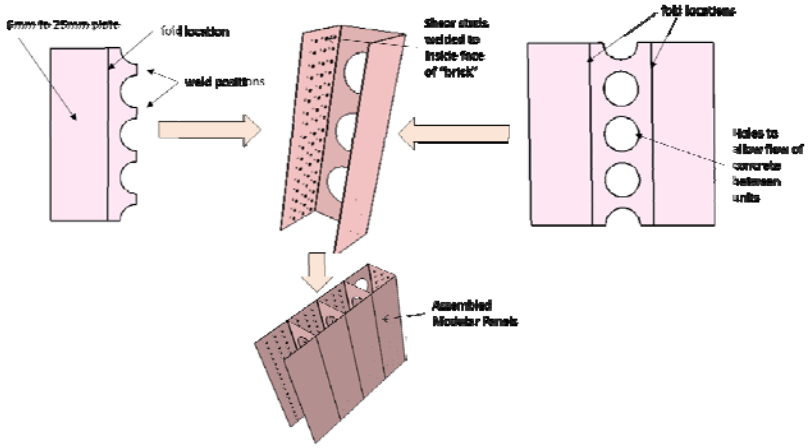

Figure 1. Fabrication and Assembly Process of Modular Panels

RELEVANT CODE EQUATIONS

The out-of-plane shear strength equations provided in AISC N690s1 (AISC, 2015) are presented in Equations (1) – (3). The nominal concrete out-of-plane shear strength contribution (V_{conc}) is given in Equation (2) and the nominal shear reinforcement contribution (V_s) is given in Equation (3). The AISC specification is applicable to shear reinforcement types that are individual components such as structural shapes, frames or bars. The out-of-plane shear strength of SC members with shear reinforcement spaced at greater than half the section thickness is calculated to be the greater of V_{conc} and V_s.

The out-of-plane flexural strength equation in the AISC N690s1 is given in Equation (4). This equation does not account for the rib contribution to the flexural strength, as for the case when the inner plates are parallel to the specimen length. Therefore, the equation developed by the authors (Sener et al., 2015), also provided in the commentary of the code provisions (Equation C-A-N9-11), were used to accurately estimate the flexural strength of SC walls by taking account of faceplate stiffener contribution .

In the equations, f'_c is the compressive strength of concrete (in ksi), t_{sc} is the SC section thickness, t_c is infill thickness of concrete, which equals to $t_{sc}–2t_p$, l is the unit width (taken as specimen width), p_S is the shear reinforcement ratio which equals to t_c/s_{tl}, where s_{tl} is the spacing of shear reinforcement along the direction of one-way shear, s_{tt} is the spacing of shear reinforcement transverse to the direction of one-

way shear, F_t is the nominal tensile strength of shear reinforcement, ξ is 1.0 for yielding reinforcement, and A_s is the cross-sectional area of faceplate in tension.

In the flexural strength equation in (5), c is calculated by Equation (6), where n is the modular ratio calculated as E_s/E_c and n' is the ratio of the plate yield strength to the concrete compressive strength, f_y/f'_c. A_{rib} is the cross-sectional area of faceplate stiffener (rib), and d_{rib} is the distance between the centroidal axes of the ribs.

$$\begin{aligned} V_{no} &= V_{conc} + V_s \quad (for\ s \le \tfrac{t_{sc}}{2}) \\ &= \max(V_{conc}, V_s) \quad (for\ \tfrac{t_{sc}}{2} < s < t_{sc}) \end{aligned} \tag{1}$$

$$V_{conc} = 0.05\sqrt{f'_c}\, t_c l \tag{2}$$

$$V_s = \xi p_s F_t (l / s_{tt}) \le 0.25\sqrt{f'_c}\, t_c l \tag{3}$$

$$M_n = f_y(A_s)(0.9t_{sc}) \tag{4}$$

$$M_{n.rib} = f_y(A_s)(d - t_p) - \tfrac{1}{2} f'_c b_w c(\tfrac{c}{3} + \tfrac{t_p}{2}) + f_y A_{rib}(\tfrac{d + d_{rib} - t_p}{2}) \tag{5}$$

$$c = 2\left[t_p\left(n' - n\right) + \tfrac{f_y A_{rib}}{f'_c b_w} \right] \tag{6}$$

The design strength equations provided in ACI 349 and Eurocode2 were developed for conventional concrete structures such as reinforced concrete structures. These equations are not directly applicable to the SC beams tested as part of this research with their specific inner-plate design, therefore are not discussed herein.

SPECIMEN DESIGN

The objectives of the beam tests were to investigate the out-of-plane shear behavior and evaluate the performance of the fabrication technique utilized to construct the specimens. The specimens were designed to fail in out-of-plane shear (with a shear span-to-depth ratio of 2.0). The two tested specimens consisted of beams with steel faceplates on the exterior surfaces acting as longitudinal reinforcement and concrete infill in between the faceplates. The steel faceplates were made from EN 10025-S355J2+n and anchored to the concrete infill using headed shear studs. The fabricated modules were welded to one another at the bent faceplate corners to assemble the specimens.

Table 1 summarizes and compares the relevant geometric parameters for the two SC beam specimens. The specimens had identical depth, faceplate and inner plate thickness, stud spacing and hole size. Specimen MWS-Type 1 had diaphragm plates that are transverse to the length of the specimen. Specimen MWS-Type 2 had two diaphragm plates running parallel to the specimen length. The width of MWS-Type 2 was twice the width of MWS-Type 1 (900 mm vs. 450 mm).

Table 1: Specimen Dimensions

Dimensions in. (mm.)	MWS-Type 1	MWS-Type2
Specimen Width (b_w)	17.7 (450)	35.4 (900)
Specimen Depth (Wall Thickness, t_{sc})	17.7 (450)	17.7 (450)
Thickness of concrete (t_c)	16.9 (430)	16.9 (430)
Thickness of faceplate (t_p)	0.39 (10)	0.39 (10)
Thickness of diaphragm (inner) plate	0.39 (10)	0.39 (10)
Transverse spacing of inner-plate (S_{tt})	N/A	17.7 (450)
Longitudinal spacing of inner-plate (S_{tl})	17.7 (450)	N/A
Spacing of studs (s_{tt}, s_{tl})	5.91 (150)	5.91(150)
Specimen Length	159 (4060)	177 (4500)
Diameter of inner-plate holes (D)	10.63 (270)	10.63 (270)

The tested beams have been designed and detailed such that: (i) the expected out-of-plane shear strength ($V_{n.exp}$) of SC beams is less than the shear force corresponding to the expected flexural capacity of the beams ($M_{n.exp}/2t_{sc}$) (for a shear span-to-depth ratio of 2.0). (ii) The interfacial shear strength of the SC beams is greater than the out-of-plane shear strength of SC walls. This has been achieved by designing the shear stud size and spacing in accordance with AISC N690s1 Sections N9.1.3 and N9.1.4 (by satisfying the faceplate slenderness and composite action requirements). In summary, the calculated out-of-plane flexural strength for the specimens is greater than the corresponding out-of-plane shear strength, and the interfacial shear strength is also greater than the out-of-plane shear strength, setting up the desired hierarchy of limit states and failure modes (out-of-plane shear failure governing) for the SC beams.

During the design process, the expected out-of-plane shear strength of the specimens was calculated using AISC N690s1 design equations, Equation (1) – (4). The tested specimens had a shear reinforcement (diaphragm plate) spacing equal to the section depth (d). Per AISC N690s1 Section N9.3.5b, for SC walls with shear reinforcement spacing larger than $d/2$, the design shear strength is limited to the greater of the steel shear reinforcement and concrete contributions. Shear reinforcement contribution (V_s) governed the design strength of specimen MWS-Type 1 ($V_{no}=V_s$). The shear reinforcement contribution was simplified to $V_s = p_s F_t$ based on the shear reinforcement spacing ($l/s_{tt}=1$) and the shear reinforcement type (yielding reinforcement, $\xi=1$) that was used for the tested beams. The shear strength equation given in the AISC specification was not applicable to Specimen MWS-Type 2, since this specimen had continuous plates (with holes) as shear reinforcement.

Testing Approach

The two SC beam specimens are representative of modular panel strips taken in two orthogonal directions. Figure 2 to Figure 5 show the top, side, and section views (including the stud and diaphragm plate layout) of the two SC wall specimens. The beam specimens were subjected to four-point bending, where the locations of load and support points are illustrated in Figure 6 and Figure 9.

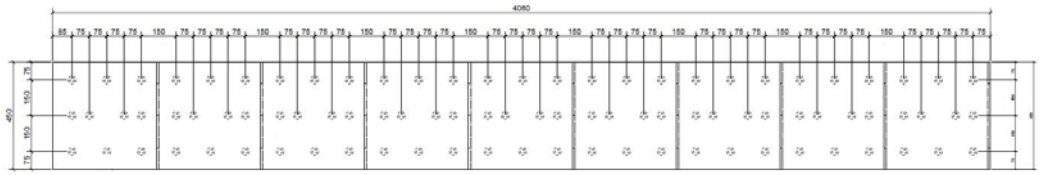

Figure 2. MWS-Type 1 – Plan (Top) View (dimensions in mm)

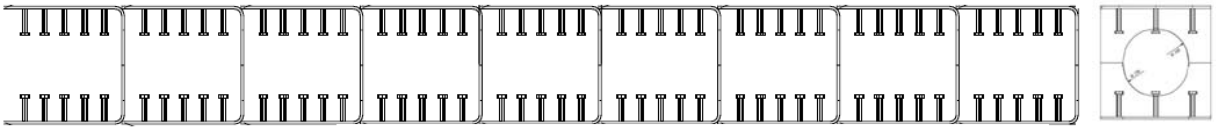

Figure 3. MWS-Type 1 – Side View and Section View (dimensions in mm)

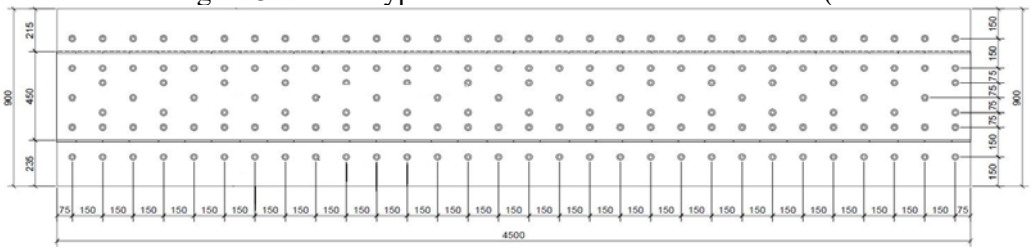

Figure 4. MWS-Type 2 – Plan (Top) View (dimensions in mm)

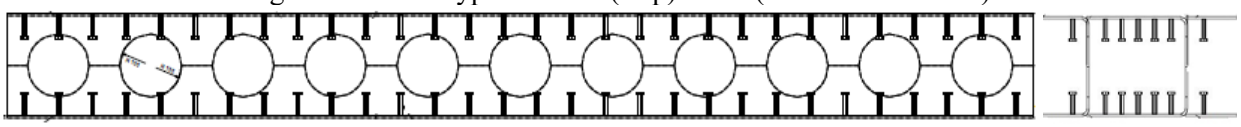

Figure 5. MWS-Type 2 – Side View and Section View (dimensions in mm)

Measured Material Properties

The concrete used for the tests was obtained from a local concrete vendor and had a maximum aggregate size of 3/4in (19 mm). The day-of-test concrete compressive strengths were obtained from testing at least three concrete cylinders. The strength for MWS-Type 1 was 4294 psi (29.61 MPa), and for MWS-Type 2 was 4329 psi (29.85 MPa).

The steel plates used for the faceplates and inner plates were from the same material. The mill test reports indicate that the plates had an average yield strength of 60.2 ksi (415.06 MPa) and tensile strength of 77.8 ksi (536.41 MPa).

Sensor Instrumentation

The response of the specimens was monitored with different types of instrumentation tools at specific locations (as shown in Figures 6 and 9). These instrumentation tools included displacement sensors, inclinometers, and strain gauges.

Displacement sensors were placed at several locations along the length of the specimen to measure vertical deflections. Support settlements were also measured using displacement sensors to calculate the chord (net) vertical deflection. Inclinometer sensors were attached to the beam cross-sections at load and support locations. The rotations that were measured under the load points allowed for the average curvature at mid-span to be calculated, which was used to develop moment vs. curvature plots for the SC beam cross-section. The support inclinometers measured the rotations of the support and demonstrated that the cylindrical support bearings performed their functions adequately.

Steel strain gauges were attached on both top and bottom steel plates along the beam length. The strain gauges on the faceplates were aligned to be on the same cross-section to evaluate section strain diagrams. The data obtained from these gauges was also used to obtain the neutral axis location. Additionally, internal strain gauges were attached to the inner (diaphragm) plates located in the shear span of the beams. These strain gauges were placed at the mid-depth and embedded in concrete after casting.

EXPERIMENTAL RESULTS

Specimen MWS-Type 1

The shear span-to-depth ratio of the specimen was set equal to 2.0 and the inner plates were oriented transverse to the specimen length for Specimen MWS-Type 1. A schematic drawing of the specimen with load and support locations is shown in
Figure 6. The test consisted of three intermediate loading and unloading cycles. The first load cycle (up to 40 kips) was conducted to obtain the elastic force-deflection behavior and stiffness for Specimen MWS-Type 1. Additionally, this force level approximately corresponded to the shear contribution of concrete (V_{conc}). The second load cycle was conducted to obtain the loading-unloading out-of-plane force deflection behavior at a load level corresponding approximately to the out-of-plane shear contribution from inner plates (V_s).

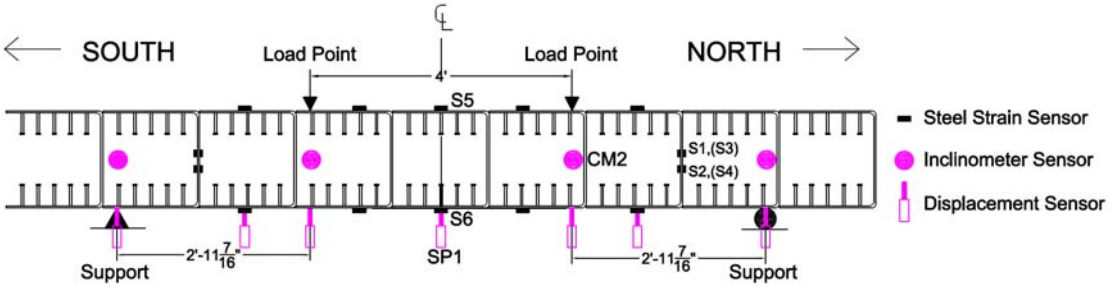

Figure 6. Specimen Drawing of MWS-Type 1

Figure 7 (a) shows the average shear force vs. mid-span displacement plot. In this figure, the average force is calculated by taking the average of the forces applied by the two hydraulic rams. The vertical deflections were measured from the chord of the specimen (straight line connecting the supports, including the support vertical deflections).The figure also includes horizontal lines corresponding to V_{conc} and V_s (=V_{no}), as presented in Equations 2 and 3 respectively. The comparison shows that the maximum measured vertical shear force from the experiment (V_{exp} =180 kips) was larger than both V_{conc} and V_s.

The force-displacement response shown in Figure 7 (a) indicates a nearly elastic response up to the peak load level. A negative post-peak slope indicates the shear failure of the specimen. Some nonlinearity was observed in the force-deflection response due to cracking of the concrete and yielding of the inner (diaphragm) plates. The specimen reached its initial peak load at 180 kips with 0.53 in. of displacement. Shear failure of the beam specimen occurred in the north shear span at this point, as shown in Figure 8. The specimen load resistance gradually reduced to 130 kips with mid-span displacement of 1.7 inches. The experiment was terminated at this point since the load capacity had reduced by more than 20%.

Figure 7 (b) shows the strain profile through the mid-span cross section at various load levels. This strain profile was developed by combining strain profiles of the faceplate steel at the mid-span cross-section (constant moment region), where the bending moment is maximum. The top (values obtained from strain gauges S5) and bottom (S6) steel plate strains at different load levels (up to the maximum shear force) were connected. The steel strain gauges indicated that the faceplates remained in the elastic range (less than ε_y = 2076 με). This also confirmed the failure mode was shear failure in concrete infill and not flexural yielding of the steel faceplates. The neutral axis of the section was about 6.5 inches from the top of the specimen, which corresponded to approximately 1/3rd of the thickness of the beam. The neutral axis calculated per Equation C-A-N9-1a of AISC N690s1 was equal to 6 inches; and was therefore consistent with the measured neutral axis obtained from the strain profile.

Figure 7 (c) shows the measured shear reinforcement strains in the failed shear span (north). The strains first increased after inclined shear (diagonal) cracking of the concrete (~50 kips), and then increased proportionally with the applied loading. The yield strain (ε_y) of the plate sections, 2076 με (i.e., 60.2 ksi/29000 ksi), was reached when the applied shear was at 160 kips, and then exceeded this level with increasing load. The diagonal cracks in concrete widened at a faster rate after the yielding of inner plates, which resulted in concrete compression strut failure that eventually caused the loss of load resistance of the beam specimen. The specimen failure state (as shown in Figure 8) indicate formation of a strut-tie mechanism. The concrete strut was at an angle of approximately 45 degrees, with cracks spanning from the load point to the adjacent shear reinforcement plate in the shear span.

Figure 7 (d) shows the section moment-curvature response, where the curvature was calculated using the rotation measured by the rotation transducer CM2. Since the rotation transducers are bonded to the concrete surface, local cracking on the surface can result in minor discrepancies in the readings. The average curvature was calculated by considering that the reading of CM3 (malfunctioned during the test) was similar to the reading from CM2, since both sensors were symmetrically located under each loading frame. The measured curvature from the rotation transducer CM2 was compared with the 2D section fiber analysis results. The estimated curvature was calculated by dividing the rotations measured at CM2 with the distance between the sensor CM2 and the mid-span (24 inches). The curvature measurements calculated from the rotation transducers were in excellent agreement with the moment-curvature response from the section fiber analysis. This confirmed that interfacial slip had negligible effect on the global stiffness response, since the 2D section fiber analysis was based on full strain compatibility through the cross-section.

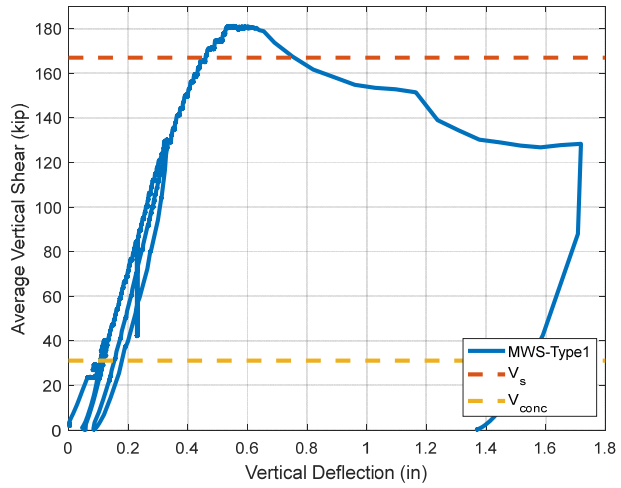

(a). Vertical Shear vs. Mid-Span Displacement

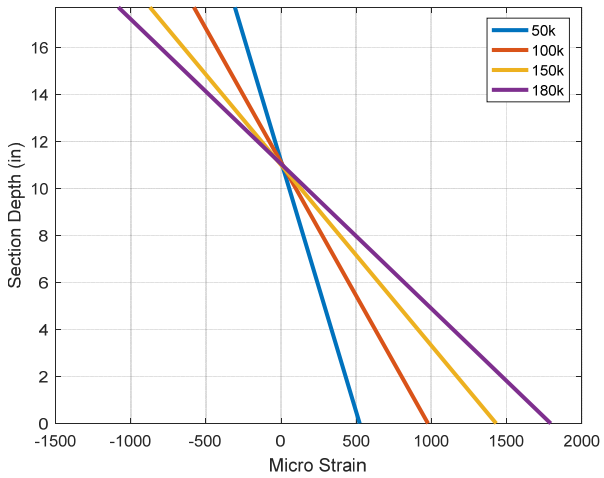

(b). Section Strains at Mid-Span (S5-S6)

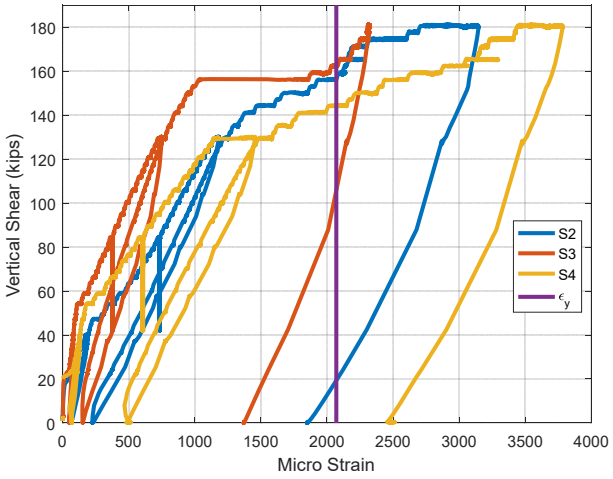

(c). North shear reinforcement strains

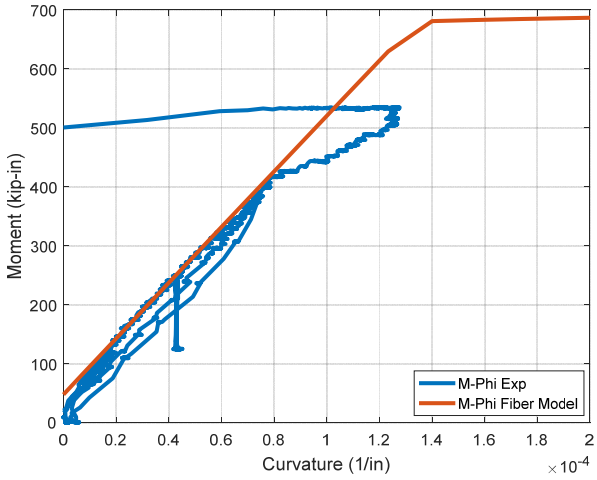

(d). Moment - Curvature

Figure 7. Specimen MWS-Type 1 Experimental Results

Figure 8. Shear Failure of MWS-Type 1 at 180 kips (North Shear Span – East Face)

Specimen MWS-Type 2

The shear span-to-depth ratio of the specimen was set equal to 2.0 and the inner plates were oriented parallel to the longitudinal span for Specimen MWS-Type 2. A schematic drawing of the specimen with load and support locations are shown in Figure 9.

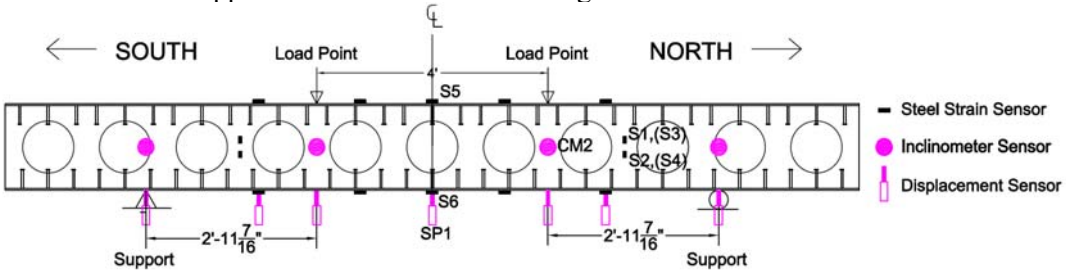

Figure 9. Specimen Drawing of MWS-Type 2

The test consisted of five load cycles. The first load cycle (corresponding approximately to V_{conc},) was conducted to obtain the elastic force-deflection behavior and stiffness of Specimen MWS-Type 2. The third load cycle was conducted to obtain the loading-unloading out-of-plane force deflection behavior at load level corresponding to V_s.

Figure 10 (a) shows the vertical shear-mid span displacement response, with horizontal lines indicating V_{conc} and V_s (=V_{no}). The response comparisons show that the maximum vertical shear force (V_{exp} =520 kips) was larger than both V_{conc} and V_s. The force-displacement response indicates a nearly elastic response until the yielding of the faceplates. The specimen reached its initial peak load at 500 kips with 0.7 inches of mid-span displacement. Flexural yielding of the specimen occurred at this point, followed by plastic (inelastic yielding) response. The applied load increased gradually to 525 kips with mid-span displacement of 1.4 inches (2 times the displacement at initial faceplate yielding). Flexural-shear failure of the beam specimen occurred in the north shear span at this point due to wide diagonal cracks. Simultaneous yielding in the inner (diaphragm) and face plates was observed prior to failure of the specimen. The force eventually decreased to 490 kips with mid-span displacement of 1.9 inches. The experiment was terminated at this point since the force capacity had reduced by about 20%.

The wide diagonal concrete crack that resulted in the failure in the north shear span is shown in Figure 11. The angle of this crack that caused the failure of specimen MWS-Type 2 was lower than the failure crack that was observed for specimen MWS-Type 1. This crack spans between the load point and support point (as shown in Figure 11).

Figure 10 (b) shows the strain profile through the mid-span cross section at various load levels. This strain profile was obtained by connecting the top (S5) and bottom steel plate (S6) strains. The strain profile indicates that the bottom faceplate exceeded the yield strain when the applied shear was greater than 400 kips. The neutral axis of the section was about 5.5 inches from the top of the specimen, which corresponded to approximately 1/3rd of the thickness of the beam. The neutral axis calculated per Equation C-A-N9-1a in AISC N690s1 was equal to 6 inches; and was therefore consistent with the measured neutral axis obtained from the strain profile.

Figure 10 (c) shows the measured strains on the inner-plate of the specimen located within the failed shear-span. As shown, the strains initiated after diagonal tension (shear) cracking of the concrete (~100 kips), and increased proportionally with applied loading. The yield strain (ε_y =2076 με) of the inner (diaphragm) plate was reached when the applied shear was at about 400 kips. The inner-plate strains increased rapidly post-yield of the plate. Since significant yielding was also observed on the faceplates, the failure mode was flexure-shear type, which is a concrete shear failure occurring after the yielding of the steel faceplates.

Figure 10 (d) shows the section average moment-curvature response, where the curvature was estimated using the rotation measured by the inclinometer CM2. The curvature estimated by the rotation

transducers CM2 is used to compare with the section fiber analysis results. The moment curvature comparisons indicate that the stiffness obtained from the experiment was slightly less than the 2D section fiber analysis, indicating that partial composite action or slip between steel and concrete layers may have influenced the response for this specimen.

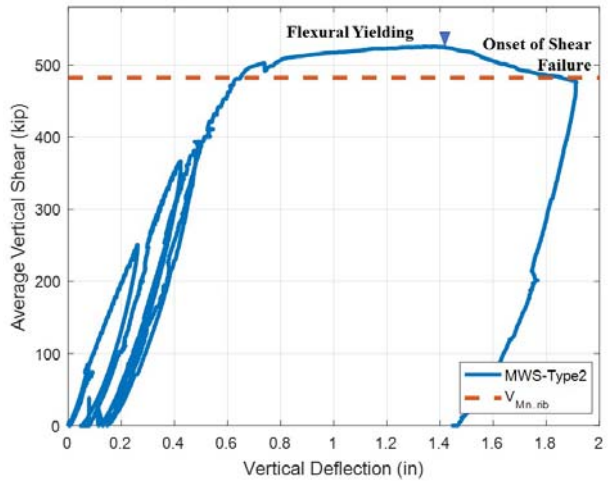

(a). Vertical Shear vs. Mid-Span Displacement

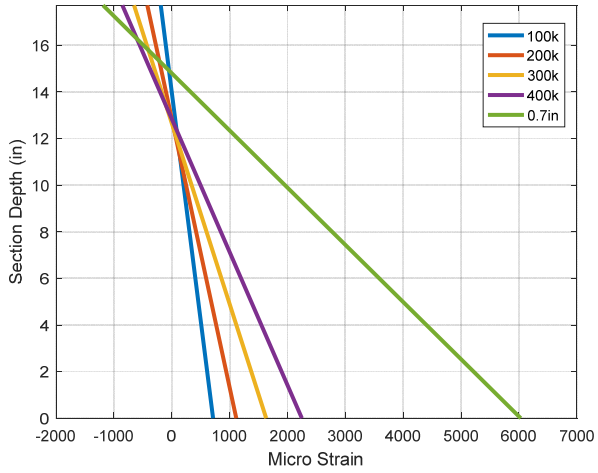

(b). Section Strains at Mid-Span (S5-S6)

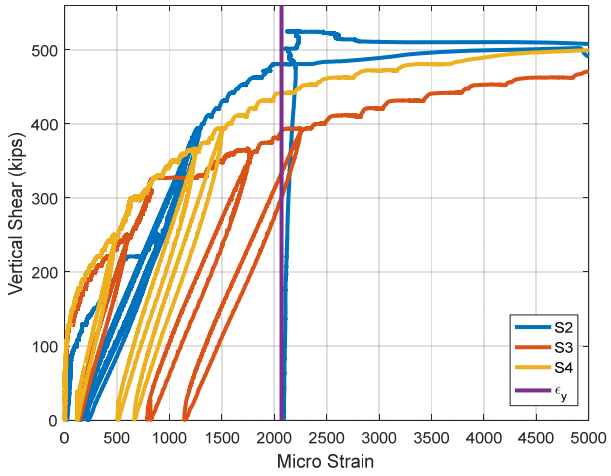

(c). North Shear Span Shear Reinforcement Strains

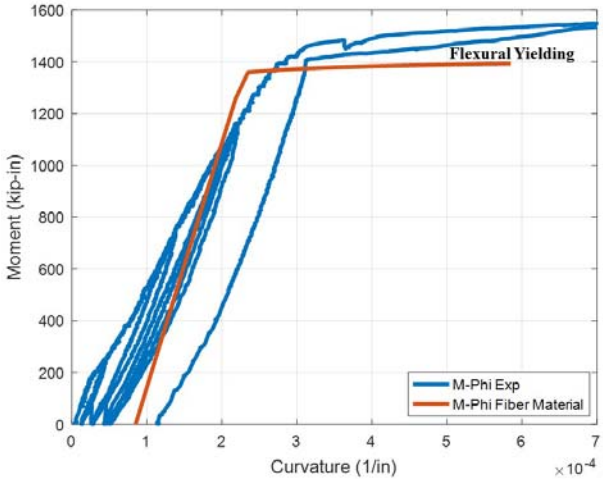

(d). Moment - Curvature

Figure 10. Specimen MWS-Type 2 Experimental Results

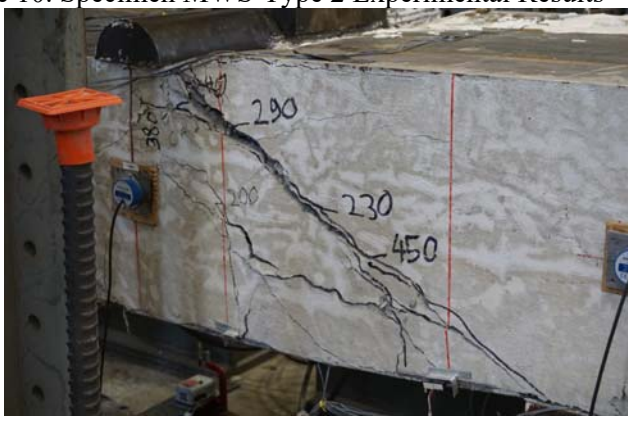

Figure 11. Shear Failure (North Shear Span – East Face) of MWS-Type 2 after Flexural Yielding

SUMMARY OF TEST RESULTS

The measured strengths for both the specimens exceeded the nominal design strengths (shear or flexure based on failure mode) calculated using the design equations provided by AISC N690s1. Table 2 below includes the comparisons between the calculated nominal strengths and the experimentally measured strength for both the specimens. As discussed previously, the AISC specification defines the shear reinforcement as ties consisting of individual components such as structural shapes, frames or bars. Therefore, these equations were not applicable to Specimen MWS-Type 2 as it possessed continuous shear reinforcement plates. Further, the AISC specification flexural strength equation (Equation 4) does not account for the flexural strength contribution of faceplate stiffeners (ribs). Therefore, Equation (5) was used to calculate the flexural capacity of MWS-Type 2, and the force corresponding to the flexural capacity (V_{Mn}) is given in the table.

The comparisons indicate that the code equations are applicable to estimate the strengths measured in the experiments. Specimen MWS-Type 1 had a shear failure before flexural yielding and the measured strength was greater than the design shear strength. The calculated flexural strength was larger than the measured strength confirming that the specimen did not experience flexural yielding before undergoing shear failure. Specimen MWS-Type 2 had a flexural-shear failure mode, where the shear failure occurred after the flexural yielding of the faceplates. The calculated shear force corresponding to the flexural strength (V_{Mn}) was within 10% of the measured strength (V_{exp}).

Table 2: Summary of Results

Specimen	MWS-Type 1	MWS-Type 2
V_{conc} (kip)	31.1	62.4
$V_s=V_{no}$ (kip)	167.4	N/A
V_{Mn} (kip)	196	482
V_{exp} (kip)	180	520
V_{exp}/V_{no}	1.08	N/A
V_{exp}/V_{Mn}	0.92	1.08

CONCLUSIONS

This paper presented experimental evaluations conducted on SC walls constructed using a novel fabrication technology. The SC specimens were subjected to out-of-plane shear loading through four-point bending test. The test specimens consisted of two beams representing orthogonal unit widths of a typical modular SC design configuration. The major difference between the specimen designs was the inner (diaphragm) plate orientations. This specimen design difference was observed in the experimental behavior and concrete cracking angle. The specimen strengths were estimated accurately and conservatively by relevant design code equations.

The novel fabrication methodology implemented in the construction of the specimens demonstrated excellent performance as there were no failures in the steel modules or the welded joints.

REFERENCES

AISC (2015). Specification for Safety-Related Steel Structures for Nuclear Facilities Including Supplement No. 1. American Institute of Steel Construction. AISC N690s1. Chicago, IL, 2015.

Sener K.C., Varma A.H. (2015). “Steel-plate composite (SC) walls: out-of-plane flexural behavior, database, and design.” Journal of Constructional Steel Research, May 2015; 108:46–59. http://dx.doi.org/10.1016/j.jcsr.2015.02.002.